NASA TECHNICAL NOTE

NASA TN D-6727

NASA TN D-6727

LAMINAR FLOW STUDIES OF A LOW-TEMPERATURE SPACE RADIATOR MODEL USING D-SHAPED TUBES

by Theodore C. Cintula, George M. Prok, and Daniel B. Johnston

Lewis Research Center
Cleveland, Ohio 44135

NATIONAL AERONAUTICS AND SPACE ADMINISTRATION • WASHINGTON, D. C. • MARCH 1972

ERRATA

NASA Technical Note D-6727

LAMINAR FLOW STUDIES OF A LOW-TEMPERATURE SPACE RADIATOR MODEL USING D-SHAPED TUBES

by Theodore C. Cintula, George M. Prok, and Daniel B. Johnston
March 1972

Page 10, equation (2): The last term on the right side should be $+T_{SINK}^4$ instead of $-T_{SINK}^4$.

Page 12, equation (10): The denominator on the right side should be μA_T instead of A_T.

Pages 30 and 31, tables III(a) and (b): The symbol for Effective radiator sink temperature, column 9, should be T_{SINK}.

Issued February 1973

1. Report No.	2. Government Accession No.	3. Recipient's Catalog No.
NASA TN D-6727		

4. Title and Subtitle	5. Report Date
LAMINAR FLOW STUDIES OF A LOW-TEMPERATURE SPACE RADIATOR MODEL USING D-SHAPED TUBES	March 1972
	6. Performing Organization Code
7. Author(s)	8. Performing Organization Report No.
Theodore C. Cintula, George M. Prok, and Daniel B. Johnston	E-6486
	10. Work Unit No.
9. Performing Organization Name and Address	112-27
Lewis Research Center National Aeronautics and Space Administration Cleveland, Ohio 44135	11. Contract or Grant No.
	13. Type of Report and Period Covered
12. Sponsoring Agency Name and Address	Technical Note
National Aeronautics and Space Administration Washington, D. C. 20546	14. Sponsoring Agency Code

15. Supplementary Notes

16. Abstract

Test results of a low-temperature space radiator model are presented. Radiator performance is evaluated with a low-thermal-conductivity fluid in laminar flow in D-shaped cross-section tubes. The test covered a Reynolds number range from 50 to 4500 and a fluid temperature range from 294 to 414 K (70^{o} to 286^{o} F). For low-temperature radiators, the fluid-to-surface temperature differential was predominately influenced by fluid temperature in laminar flow. Heat transfer and pressure drop for the radiator tube could be predicted within engineering accuracy from existing correlations.

17. Key Words (Suggested by Author(s))

Space radiators
Laminar flow
Heat transfer
Space missions

18. Distribution Statement

Unclassified - unlimited

19. Security Classif. (of this report)	20. Security Classif. (of this page)	21. No. of Pages	22. Price*
Unclassified	Unclassified	32	$3.00

* For sale by the National Technical Information Service, Springfield, Virginia 22151

LAMINAR FLOW STUDIES OF A LOW-TEMPERATURE SPACE RADIATOR MODEL USING D-SHAPED TUBES

by Theodore C. Cintula, George M. Prok, and Daniel B. Johnston

Lewis Research Center

SUMMARY

To obtain experimental data applicable to the design of a heat-rejection radiator for the Brayton Power System, a study was made of a small-scale radiator. This report presents the results of that study. The design of the small-scale radiator was selected to represent the Brayton system radiator, and it was operated under vacuum and thermal conditions simulating low earth orbit. During the investigation, the fluid Reynolds number and the temperature were varied from 50 to 4500 and 294 to 414 K (70° to 286° F), respectively.

In laminar flow, the bulk-fluid-to-radiator-surface temperature differential was found to be predominately influenced by fluid temperature rather than Reynolds number. Low fluid temperatures resulted in low heat-rejection rates per unit area and a low temperature drop from the fluid to the radiating surface.

In the nonlaminar flow regime, both Reynolds number and fluid temperature influence the bulk-fluid-to-radiator-surface-film-temperature differential. Operation in this flow regime results in higher heat-rejection rates and larger pressure requirements.

Fin effectiveness for the test radiator was extremely high for all temperatures considered. The radiator geometry was also very responsive to sudden fluid temperature changes. Heat transfer and pressure drop for the radiator tube can be predicted within engineering accuracy from existing correlations.

INTRODUCTION

The Lewis Research Center is developing the closed-loop Brayton cycle powerplant with the ultimate intent of providing high-capacity reliable electric power for extended space missions (ref. 1). Over 2500 hours of testing at design operating conditions have been accumulated on the developmental power system. This test program used an

electric heat source in place of an isotope or nuclear heat source and a facility heat exchanger in place of a radiator for cycle waste energy rejection.

The next step in the development of a complete electrical power generating package is to provide a space-compatible heat-rejection system. To conform to a typical space mission, a circumferential tube radiator for 6.6-meter (260-in.) diameter spacecraft has been designed and is being prepared for testing (ref. 2). The finalized radiator design will use a low-thermal-conductivity silicone oil in laminar flow with a Reynolds number of approximately 500. The tube flow passages will be of D-shaped cross section.

To obtain experimental data useful in designing low-temperature radiators, a small-scale-radiator test program was completed at the Space Power Facility. The small-scale configuration is capable of simulating orbital conditions of space vacuum and sink temperature. The small-scale radiator is typical of, but not identical to, the actual radiator. Primary differences are in tube and fin dimensions. The small-scale radiator is not armored. However, the small radiator uses the same radiator fluid, and the tube geometry is also D-shaped.

The area of investigation for the small-scale-radiator program is to provide experimental data useful for low-temperature-radiator design. Also, the data can be used for substantiating and improving computer design programs where limited information is available. Specifically, this would include

(1) Study present low-temperature-radiator performance

(2) Evaluate bulk-fluid-to-radiator-surface-temperature differential for a low-thermal-conductivity fluid in laminar flow

(3) Confirm pressure drop predictions for laminar flow in D-shaped cross-section tube

(4) Confirm the radiator computer program design point

This report discusses the results of these tests at a variety of radiator temperatures and flow conditions for a single radiator geometry.

TEST APPARATUS

A complete schematic of the test system is shown in figure 1. This figure shows the cross-sectional arrangement of the vacuum chamber, the radiator, and the cold wall.

Radiator Panel Description

The radiator panel is made of laminated aluminum sheets with integrally formed tubes. The radiator is illustrated in figure 2. Overall dimensions of the model radiator are 2.42 meters by 0.84 meter (96 in. by 33 in.). The radiator is formed by bonding

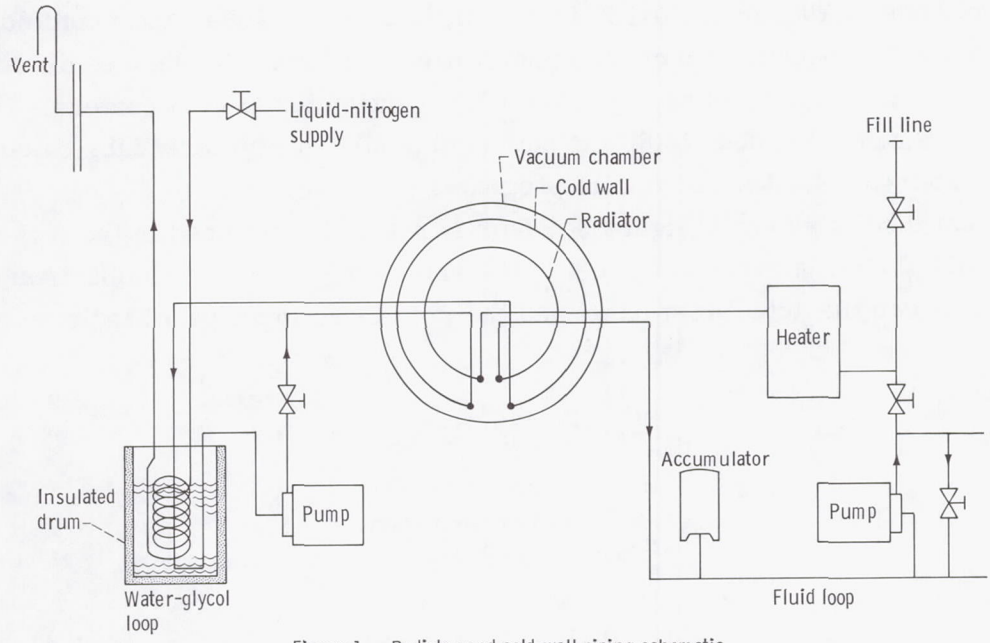

Figure 1. - Radiator and cold-wall piping schematic.

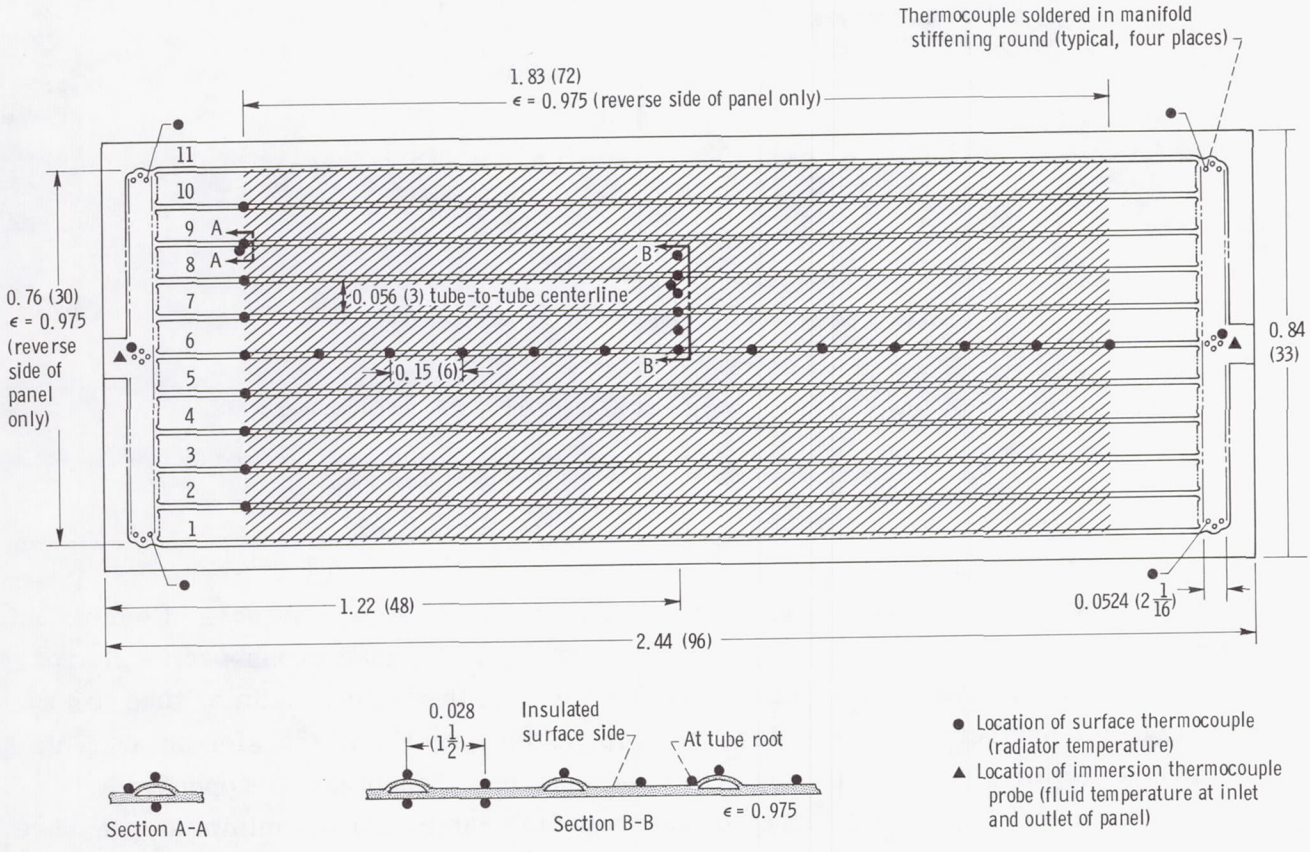

Figure 2. - Radiator panel dimensions and thermocouple locations. All nonshaded areas are insulated. Dimensions are in meters (in.).

under heat and pressure two separate 1100 series aluminum sheets of approximately 1.52 and 0.76 millimeter (0.060 and 0.030 in.) final thickness. Tubes and manifolds are not bonded and are subsequently formed by pneumatic inflation to the desired dimensions. The model radiator has 11 tubes, spaced on 7.6-centimeter (3-in.) centers. Nominal working pressure of the tubes is 689 kN/m^2 (100 psia). A similarly fabricated diffusion-bonded radiator was used in the Apollo program.

A typical tube is shown in figure 3. This is not a channel used in the test radiator but one obtained from a sectioned panel of the same lot. Exterior comparison of tube dimensions between the actual test panel and the cross-sectioned panel indicate that channel

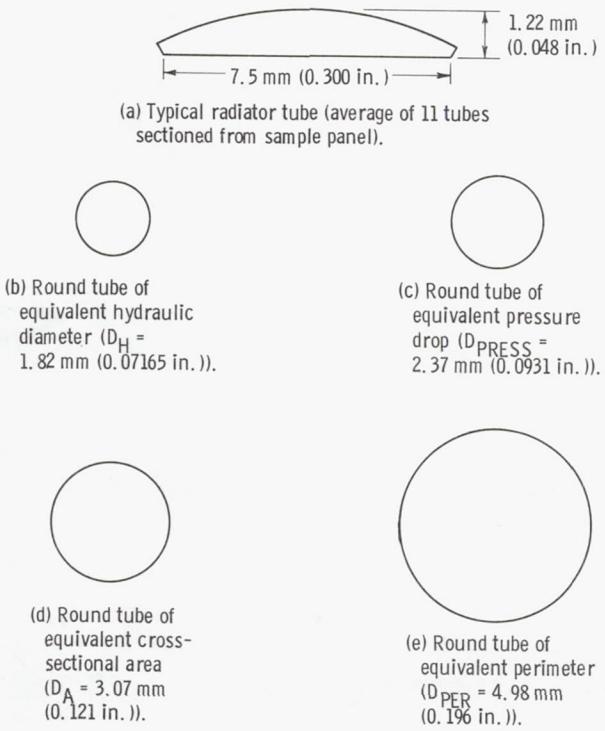

Figure 3. - Typical radiator tube and respective equivalent round tubes. All sketches are in 5:1 scale.

dimensions are representative. Also shown in figure 3 are four round tubes of equivalent dimensions and pressure drop. Comparing the round tube of equal cross-sectional area (fig. 3(d)) to the other tubes shown in figure 3 shows that the typical radiator tube has a lower Reynolds number, a higher pressure drop, and a larger heat transfer area. This condition exists for all nonround-tube cross sections and is explained in appendix A.

The tube manifolds were designed by the manufacturer to provide minimum pressure loss and equivalent tube flow (fig. 2). The manifolds terminate in 25.4-millimeter (1-in.) outside-diameter tubing.

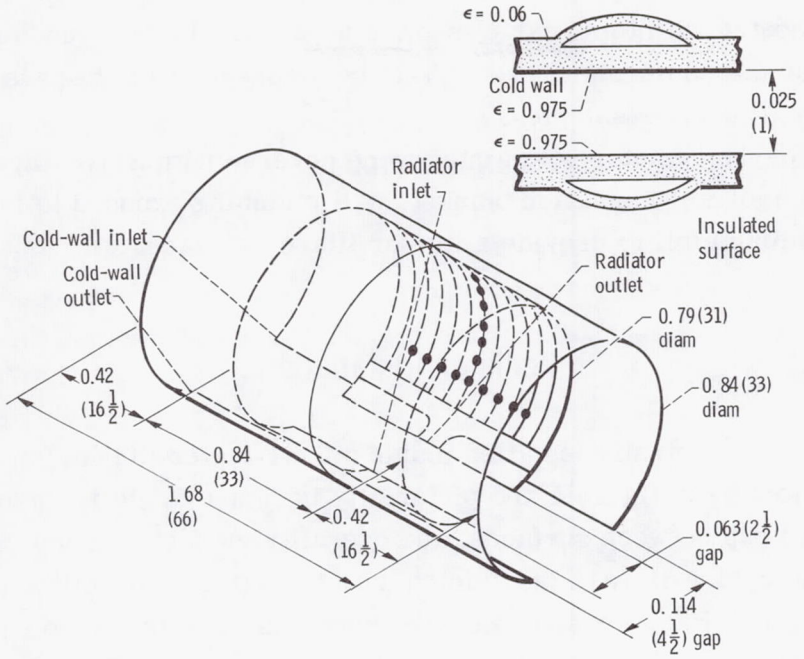

Figure 4. - Radiator panel as centrally installed in cold wall. Dimensions are in meters (in.).

The radiator panel was rolled into a 0.79-meter (31-in.) diameter, as shown in figure 4. It was eventually centered in a 0.84-meter (33-in.) diameter cold wall in the vacuum chamber.

Instrumentation

To adequately map the test article, the radiator was instrumented with 20 American Wire Gage, 0.81-millimeter copper-constantan surface thermocouples, as shown in figure 2. Surface thermocouples were attached to the panel by soldering. Fluid temperature measurements were taken with exposed junction thermocouple probes inserted into mid-stream of the radiator panel inlet and outlet tubes. A detailed listing of all system instrumentation is shown in table I.

High-Emittance Coating and Insulation

A 1.83- by 0.76-meter (72- by 30-in.) centrally located area on the flat side of the panel was selected as the test radiator section. The intent was to make this area radiate as much as possible while making the remainder of the panel and exposed piping poor radiant surfaces.

The test area was spray painted with a optically black, high-emittance enamel. Duplicate samples coated with this enamel showed a reflectance of below 5 percent at a wavelength of less than 8 micrometers. Total hemispherical emittances of 0.97 and 0.98 were measured on two other samples.

All portions of the radiator not painted were covered with a five-layer, aluminized Mylar-Dexiglass multifoil insulation blanket. All plumbing exposed to the radiator was covered with aluminum foil to provide a low-emittance surface.

Radiator Installation

The radiator was centrally installed inside a 0.84-meter (33-in.) diameter cold wall, as shown dimensionally in figure 4 and pictorially in figure 5. With an approximate 25.4-millimeter (1-in.) gap between surfaces, the overall view factor is unity. The entire inner surface of the cold wall was also painted with the same high-emittance coating as the radiator test section. Radiator and cold-wall supports were insulated to minimize conductive heat transfer.

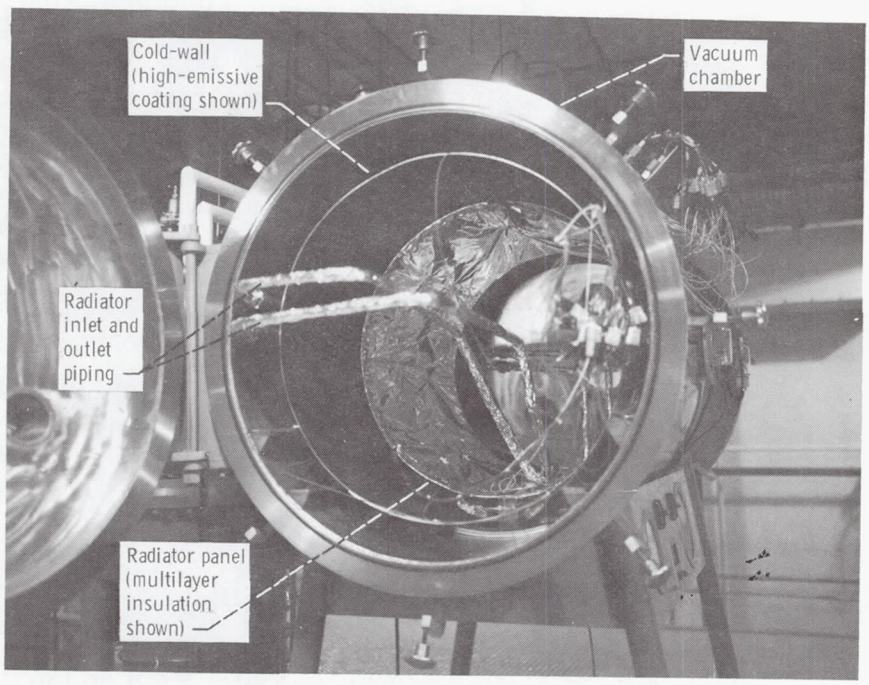

Figure 5. - Radiator and cold wall as installed in vacuum chamber.

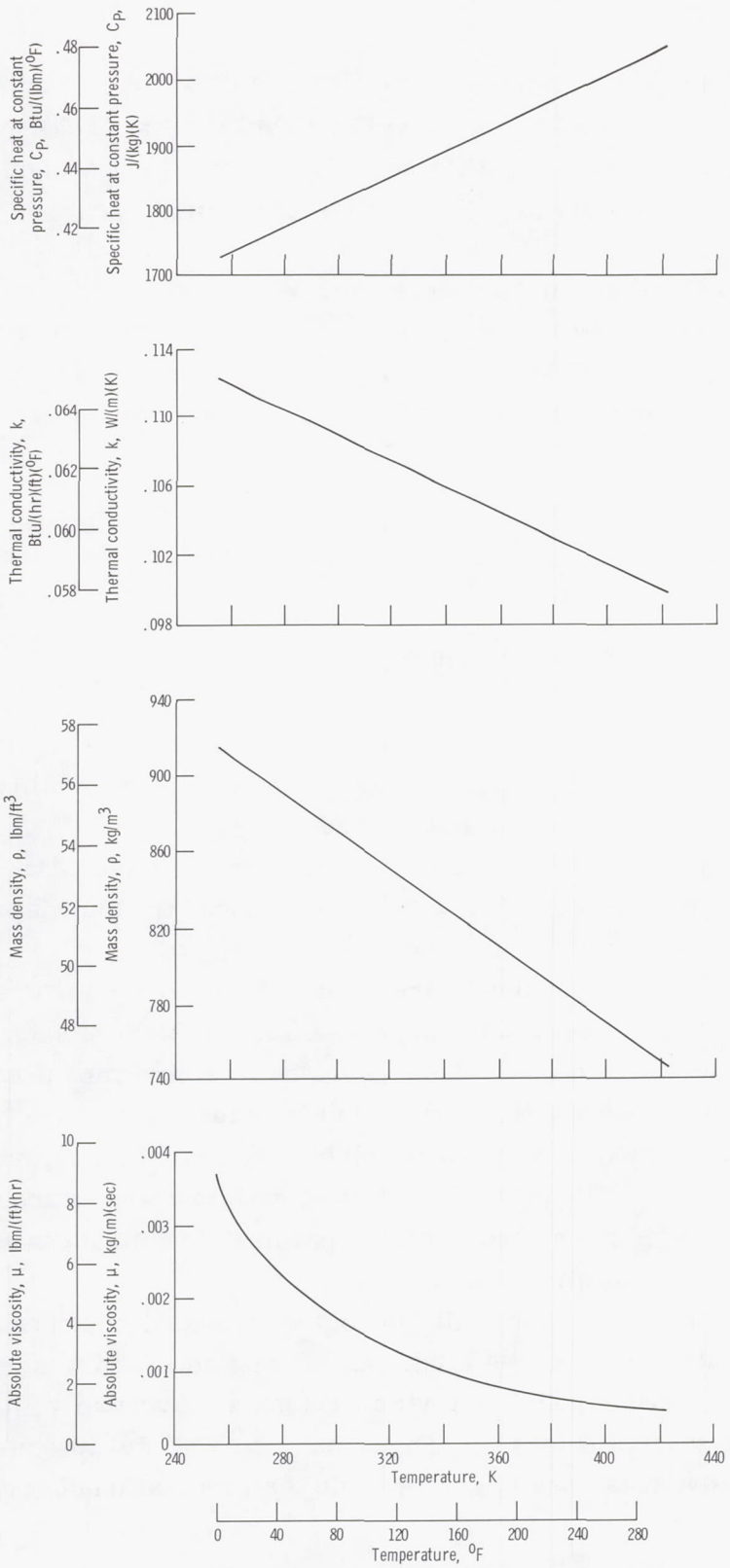

Figure 6. - Variation of radiator fluid properties with temperature.

Radiator Fluid

The radiator fluid was a silicone oil, chemically a dimethyl siloxane polymer. It is also the fluid used for waste heat rejection with the facility heat exchanger in the previous Brayton cycle testing (ref. 1) and is specified for the flight design. Temperature variation of fluid parameters used for the small-scale-radiator test program are illustrated in figure 6.

Two different test samples of fluid were used in the panel tests - one which had accumulated 2500 hours of testing in the Brayton test program, and a new fluid directly from the container. The new fluid testing was done at two identical test points as established by the old fluid to investigate any change in radiator performance caused by degradation of the fluid.

TEST PROCEDURE

Steady-State Tests

The radiator and associated plumbing were initially filled by evacuating the loop and backfilling with fluid. This minimized air entrapment and the possibility of pump cavitation and ensured that the radiator was full of fluid.

The vacuum chamber was continuously pumped over a 3-month data acquisition period. With chamber pressures in the low 10^{-7}-torr range, the multilayer insulation was thoroughly evacuated for minimum heat leak.

Ambient readings of all instrument parameters were taken prior to any test sequence. All ambient thermocouple readings were within ±0.3 K (±1/2° F) of each other, and were therefore not corrected in the reduced data. Turbine flowmeter and pressure transducers drifted slightly and were accounted for in the reduced data.

The cold wall was chilled by a pump-circulated, closed-system, water-glycol mixture, as shown in figure 1. The prime objective of each test was to acquire data at steady-state thermal equilibrium conditions. A parametric data-mapping profile for the radiator test program is shown in table II.

The basic test procedure was to chill the cold wall, establish approximate desired flow in the radiator loop, and heat the fluid. As the test condition was approached, flow rate and heater power were adjusted in finer increments. Eventually, total system heat input reached total system heat losses. The radiator was at steady-state equilibrium. A total of three successive data readings were made for verification of equilibrium.

Transient Test

One test was performed to obtain preliminary information on the response of a chilled radiator to a warm fluid. The radiator fluid was heated under no-flow conditions to a nominal temperature of 394 K (250° F) in the radiator loop reservoir. The radiator was chilled to a nominal temperature of 261 K (10° F) by exposure to the cold wall. At a preset flow rate, the warm bulk radiator fluid was circulated through the radiator. The test was terminated when steady-state radiator conditions were reached.

TEST ANALYSIS AND COMPUTATIONS - STEADY-STATE TESTS

Steady-state tests were made at a specific fluid temperature and given flow rate. To

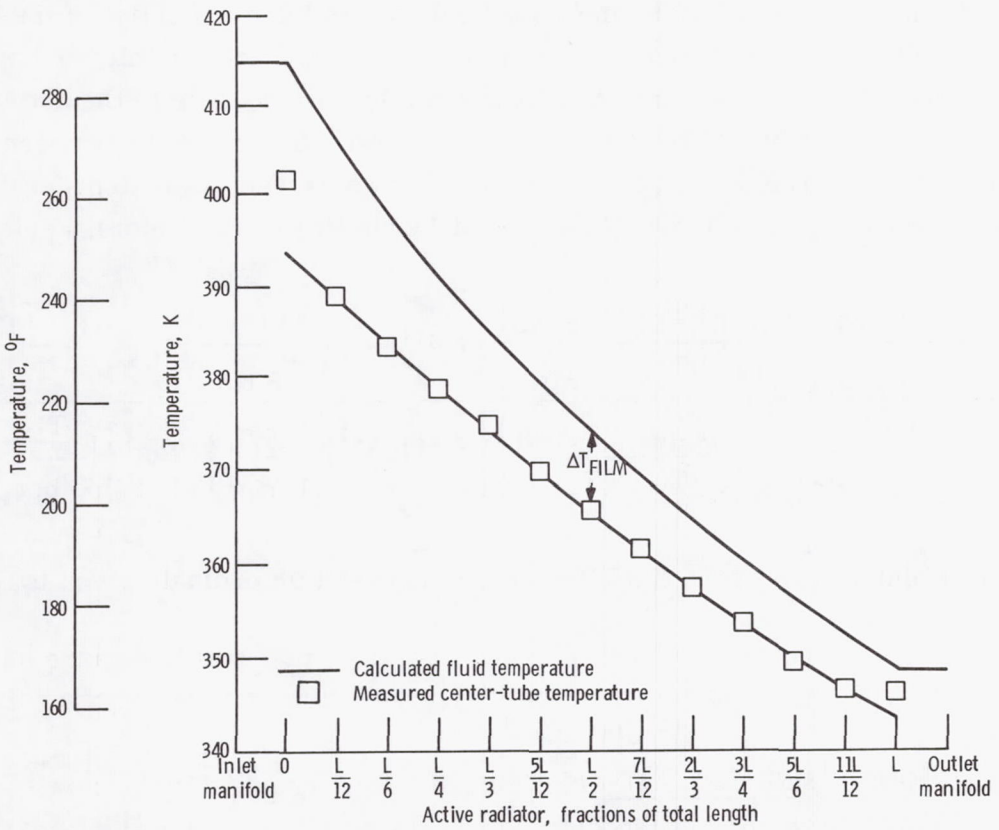

Figure 7. - Radiator fluid and center-tube temperature profiles at low Reynolds number. Flow rate, 6.69 cm^3/sec (0.106 gal/min); cold-wall temperature, 257.74 K (4.27° F). Radiative effective temperatures: of radiative fluid T_{EFF}, 377.77 K (220.32 °F); of center-tube surface T_{CT}, 366.5 K (200° F); of radiative surface T_{RAD}, 363.9 K (195.3° F); bulk-fluid-to-radiator-tube-surface temperature differential ΔT_{FILM} at L/2, 264.7 K (16.5° F). Heat transfer: total heat rejected Q, 902 W (3077 Btu/hr); heat transfer coefficient h, 300 W/(m^2)(K) (or 52.8 Btu/(hr)(ft^2)(°F); efficiency η, 82.3. Reynolds number at bulk fluid temperature, 173.

evaluate radiator performance, a plot of radiator center-tube temperature and fluid temperature profile was made for each test point, as illustrated in figure 7.

Before examining these curves, three points of prime importance should be defined. The definitions make analysis easier.

(1) T_{RAD} - The effective temperature of the entire radiative surface: It is the temperature of a uniform-temperature radiator with the same heat-rejection rate as a nonuniform temperature radiator.

(2) T_{EFF} - The effective temperature of the radiative fluid: it may be similarly defined as the uniform temperature of the fluid with the same radiant heat-rejection rate as a nonuniform temperature fluid.

(3) T_{CT} - The effective temperature of the instrumented radiative center-tube surface: It is defined analogously to T_{RAD} and T_{EFF} specifically for the center-tube temperature profile.

The upper curve shown in figure 7 is the fluid temperature distribution along the panel. Fluid temperatures could be measured only at the inlet and outlet of the manifold. These temperatures were assumed to be those of the active-radiator inlet and outlet. This assumption is premised on zero heat leak from the panel edges to the active radiator surface as this area is covered by the insulation blanket. The curve fit between the inlet and outlet of the active radiator is generated by a known-rate-of-radiation-decay curve (private communication from James P. Couch of Lewis Research Center). This curve is

$$\frac{X}{L} = \frac{\ln\left[\frac{(T_{FLUID} + T_{SINK})(T_{IN} - T_{SINK})}{(T_{FLUID} - T_{SINK})(T_{IN} + T_{SINK})}\right] + 2\left[\tan^{-1}\left(\frac{T_{FLUID}}{T_{SINK}}\right) - \tan^{-1}\left(\frac{T_{IN}}{T_{SINK}}\right)\right]}{\ln\left[\frac{(T_{OUT} + T_{SINK})(T_{IN} - T_{SINK})}{(T_{OUT} - T_{SINK})(T_{IN} + T_{SINK})}\right] + 2\left[\tan^{-1}\left(\frac{T_{OUT}}{T_{SINK}}\right) - \tan^{-1}\left(\frac{T_{IN}}{T_{SINK}}\right)\right]} \quad (1)$$

The effective temperature of the fluid lies on this curve at an ordinate given by:

$$T_{EFF} = \sqrt[4]{\frac{4T_{SINK}^3(T_{IN} - T_{OUT})}{\ln\left[\frac{(T_{OUT} + T_{SINK})(T_{IN} - T_{SINK})}{(T_{OUT} - T_{SINK})(T_{IN} + T_{SINK})}\right] + 2\left[\tan^{-1}\left(\frac{T_{OUT}}{T_{SINK}}\right) - \tan^{-1}\left(\frac{T_{IN}}{T_{SINK}}\right)\right]} - T_{SINK}^4} \quad (2)$$

where temperatures in equations (1) and (2) are in degrees absolute. (All symbols are defined in appendix B.)

Elimination of sink temperature greatly simplifies the derivation and final form of

each equation. However, in any radiator where the fluid outlet temperature approaches the sink temperature, the sink temperature will become influential. For radiative heat transfer, T_{EFF} will always be cooler than the average fluid temperature, and X/L at T_{EFF} will always be less than one-half of the active radiator length.

The calculated fluid temperature curve in figure 7 represents the operating temperature profile of a prime radiator; that is, a radiator with no film or fin losses, a 100-percent-efficient radiator. The lower curve is the temperature profile of the center radiator tube surface (tube 6). It is formed by connecting individual temperature readings with a smooth curve. Temperatures not fitting the smooth curve were simply disregarded. This always occurred at the inlet and outlet of the active radiator surface. These two end thermocouples always read slightly warmer than the smooth curve fit. This was probably caused by the mass of the insulated section of the panel reaching fluid temperatures at steady-state conditions. This provided a slight conductive heat transfer path which was detected by these thermocouples, resulting in slightly elevated temperatures. Similarly, the mid-panel thermocouple often read low as the close proximity of thermocouples at this point was somewhat of a fin effect to the cold wall.

The measured radiator center-tube temperature profile correlated almost exactly to equations (1) and (2) with appropriate substitutions of inlet and outlet temperatures. This indicates that both the equation and the test data are accurate. The effective temperature of this curve is designated T_{CT}.

The difference between the fluid temperature curve and the center-tube curve is the film temperature drop at any point. These two curves approach each other with decreasing radiator temperature, indicating that

$$\Delta T_{FILM} \propto T \tag{3}$$

The ΔT_{FILM} was evaluated only at mid-radiator for each test condition and is now defined as the temperature difference graphically measured from the two smooth curve fits shown in figure 7.

To determine the actual heat radiated, it is necessary to find T_{RAD}. The heat loss of the fluid being equivalent to heat radiated under steady-state conditions was tempered somewhat by the manifold heat conduction previously mentioned. To minimize this anomaly it was postulated that

$$T_{RAD} = CT_{CT} \quad \text{where } C < 1 \tag{4}$$

A representative temperature distribution existed at the radiator discharge (fig. 2). Discharge tube temperatures continuously decreased with distance from the center tube. This was probably caused by slightly unequal flow in each tube resulting from a manifold

pressure gradient. The constant C is the ratio of the mean discharge tube temperature to the discharge temperature of the center tube. The range of C was from 0.98 to 0.995 for the warmest to coolest radiator temperatures, respectively.

To find the total heat rejected

$$Q = FA\sigma\left(T_{RAD}^4 - T_{SINK}^4\right) \tag{5}$$

the overall heat transfer coefficient is determined by

$$h = \frac{Q}{11(PER)L\ \Delta T_{FILM}} \tag{6}$$

The overall radiator efficiency may be computed from

$$\eta = \frac{T_{RAD}^4 - T_{SINK}^4}{T_{EFF}^4 - T_{SINK}^4} = \frac{A'}{A} \tag{7}$$

Prime radiating area is

$$A' = 1.39\ m^2(\eta) = 15\ ft^2(\eta) \tag{8}$$

The D-shaped tube cross section, for engineering purposes, is converted to a hydraulic diameter defined as

$$D_H = \frac{4 \times \text{Tube cross-sectional area}}{\text{Tube perimeter}} = \frac{4A_T}{PER} \tag{9}$$

Reynolds number, based on hydraulic diameter, is now defined as

$$Re = \frac{VD_H\rho}{\mu} = \frac{W_T D_H}{A_T} \tag{10}$$

The Nusselt number is also based on hydraulic diameter; that is, $Nu = hD_H/k$. All parameters involving a representative fluid temperature for the panel were evaluated at T_{EFF}.

Panel pressure drop was measured with strain-gage-type pressure transducers located at the inlet and outlet headers. The active radiator pressure drop to total panel pressure drop was construed as the ratio of respective tube lengths. No losses were at-

tributed to the manifolds or to entrance effects, as the manifolds were designed for minimum pressure drop. The standard equation for friction factor in laminar flow is

$$f = \frac{16}{Re} \tag{11}$$

RESULTS AND DISCUSSION

Steady-State Tests

For reference, a summary of measured radiator performance parameters is listed in table III. This table lists only the tests performed with the fluid used in the Brayton test program because the two tests performed with new fluid gave identical results, indicating that the fluid did not degrade. The cold-wall temperature ranged from 253.6 to 262.4 K (-3.2° to 12.4° F) with a mean of 257.8 K (4.3° F). Data reduction and performance plotting of all information in this report was based on a total hemispherical emittance of 0.93, which is the manufacturer's published value, rather than on the average measured value of 0.975 obtained under laboratory conditions on a 25.4-millimeter (1-in.) square sample. It was felt that the published value was more representative of the actual emittance of a large panel.

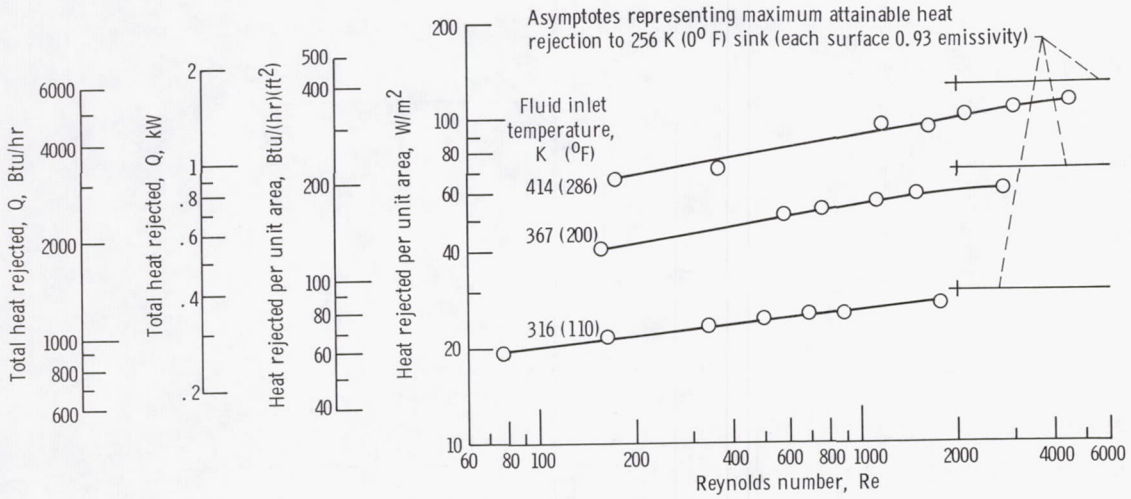

Figure 8. - Heat rejected as function of Reynolds number at various fluid inlet temperatures.

General Radiator Heat Transfer

The maximum amount of heat that can be transferred by a radiator is limited by the fluid operating temperature, specifically T_{EFF}. For the radiator to approach the maximum heat-rejection rate, the fluid-to-outer-tube-surface temperature difference and the radiator fin temperature drop must be small. It is desired to have T_{RAD} approach T_{EFF} as much as possible within design limits and practicalities.

Figure 8 shows the variation of radiator panel heat-rejection rate for different fluid inlet temperatures as a function of Reynolds number. In this figure, T_{EFF} decreases with decreasing Reynolds number on a constant fluid inlet temperature curve. Clearly, the higher the effective fluid temperature, the greater the heat rejected for a particular radiator geometry at a particular sink temperature.

The difference between effective fluid temperature and effective radiator surface temperature is illustrated in figure 9. Obviously, for a given effective fluid temperature, higher effective radiator temperatures occur at higher Reynolds number. However, this

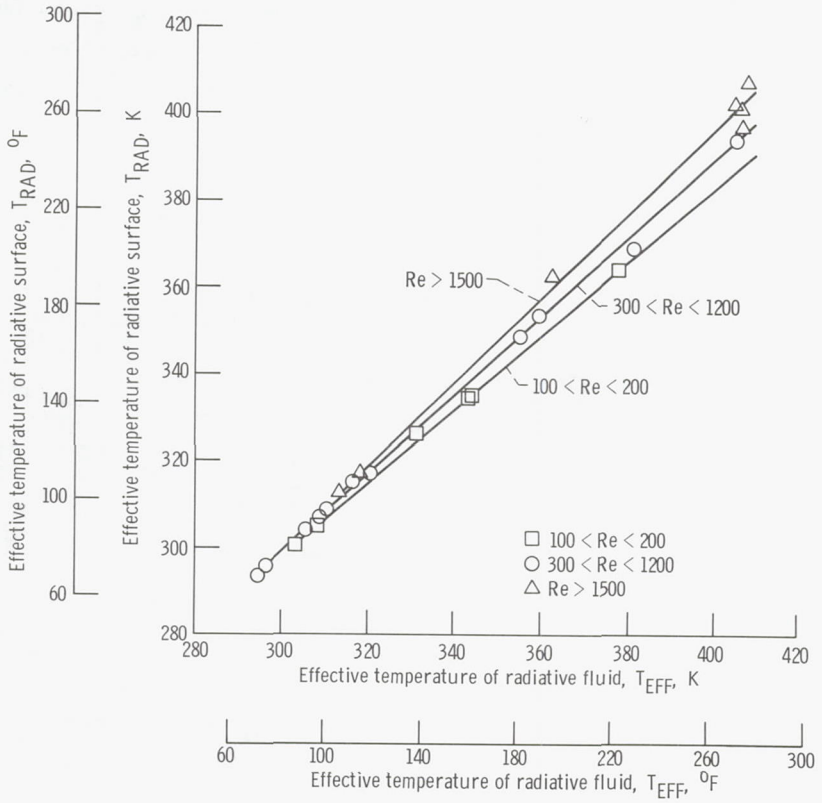

Figure 9. - Effective radiator temperature as function of effective fluid temperature at various Reynolds numbers.

effect is most minor at the lower temperatures. Efficient low-temperature radiators may be designed without regard to flow turbulence being established.

Influence of ΔT_{FILM} on Heat Transfer

Part of the difference between T_{FLUID} and T_{RAD} can be attributed to the temperature difference between the bulk fluid and the tube surface ΔT_{FILM}. The influence of

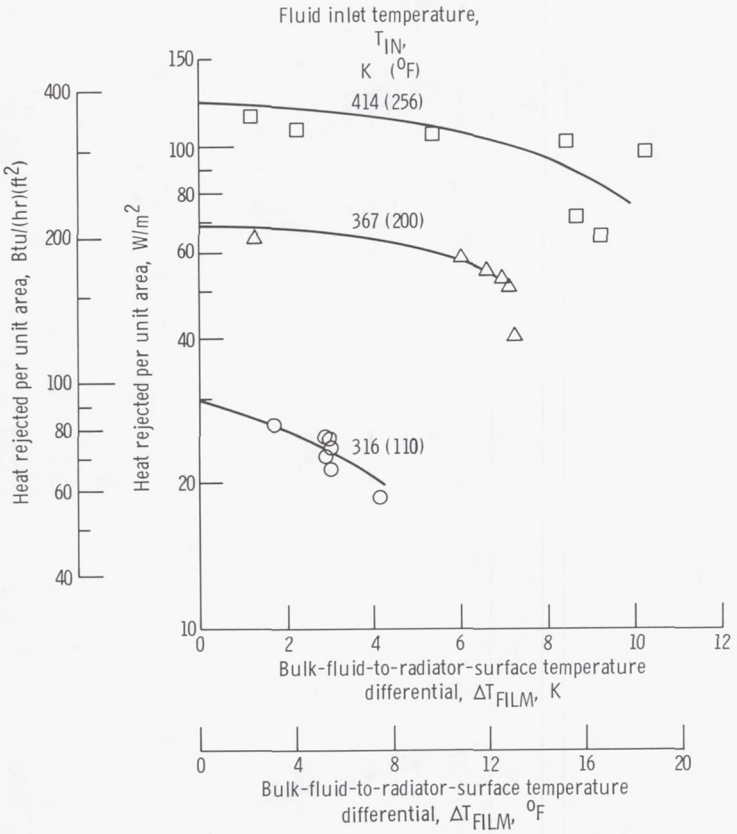

Figure 10. - Correlation between heat rejected and bulk-fluid-to-radiator-surface temperature differential at various fluid inlet temperatures.

this parameter on heat-rejection rate is shown in figure 10. As would be expected, higher temperature drops are associated with higher fluid temperatures. At a given film temperature drop, the proportional heat-rejection rate of the low-temperature fluid decreases most severely. Obviously, a low-temperature radiator cannot tolerate a large ΔT_{FILM} and be efficient.

The parameters that influence ΔT_{FILM} are the fluid temperature, the Reynolds number, and the fluid thermal conductivity. For this radiator configuration and fluid in

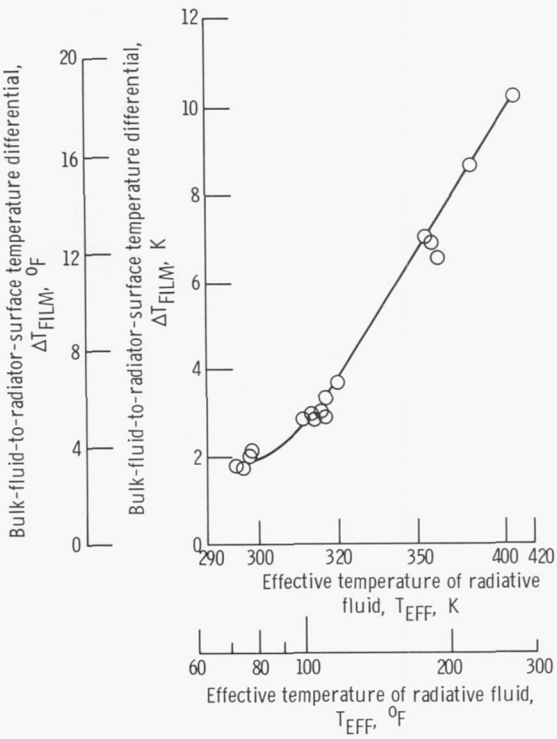

Figure 11. - Bulk-fluid-to-radiator-surface temperature differential as function of fluid temperature. Reynolds number range, 300 to 1200.

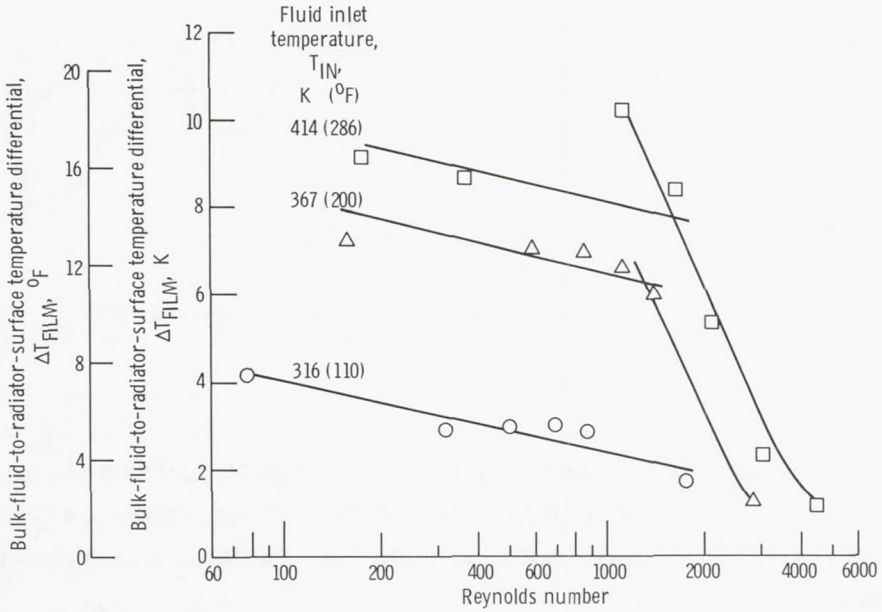

Figure 12. - Bulk-fluid-to-radiator-surface temperature differential as function of Reynolds number at various fluid inlet temperatures.

the fully developed laminar flow range, it was possible to isolate ΔT_{FILM} as a function of fluid temperature, as shown in figure 11. The straight-line portion of this curve corresponds to

$$\Delta T_{FILM} = \frac{\ln T_{FLUID} - \ln 70}{\ln 1.077} \tag{11}$$

The influence of Reynolds number on ΔT_{FILM} for the entire flow range is shown in figure 12. The curves for 414 and 367 K evidence sharp decreases in ΔT_{FILM} beginning at Reynolds number of 1200 to 1600. As will be confirmed later by another independent parameter, this represents the transition to nonlaminar flow.

Because T_{EFF} decreases with Reynolds number, the relative flatness of the curves in the laminar flow range indicates that variation of Reynolds number has very little influence on ΔT_{FILM}. In the nonlaminar flow range, sharp reductions in ΔT_{FILM} occur with increasing Reynolds number. In this flow region, ΔT_{FILM} is clearly influenced by both fluid temperature and Reynolds number. The effect of Reynolds number is sufficient to produce smaller values of ΔT_{FILM} despite higher fluid temperatures.

Radiator Fin Effectiveness

For this particular radiator geometry, temperature gradients along the radiator fin were very small. This is attributed to the high thermal conductivity of the aluminum fin material and the relatively high thickness-to-length ratio of the fin. Temperature drops between the tube surface and the tube root were within thermocouple accuracy limits and are not presented. The maximum temperature drop between the tube root and mid-fin was less than 1.1 K (2^{o} F). This occurred at maximum tube-root temperature and appeared to decrease linearly with decreasing tube-root temperatures. For this radiator configuration, temperature losses are predominantly a film effect rather than a fin effect.

Heat Transfer Coefficient

The heat transfer coefficient is shown plotted against Reynolds number in figure 13. In laminar flow, its value increases only moderately with increasing Reynolds number. In nonlaminar flow, where a slightly higher total heat rejection is combined with sharply reduced values of ΔT_{FILM}, the curve rises steeply. Taking the heat transfer coeffi-

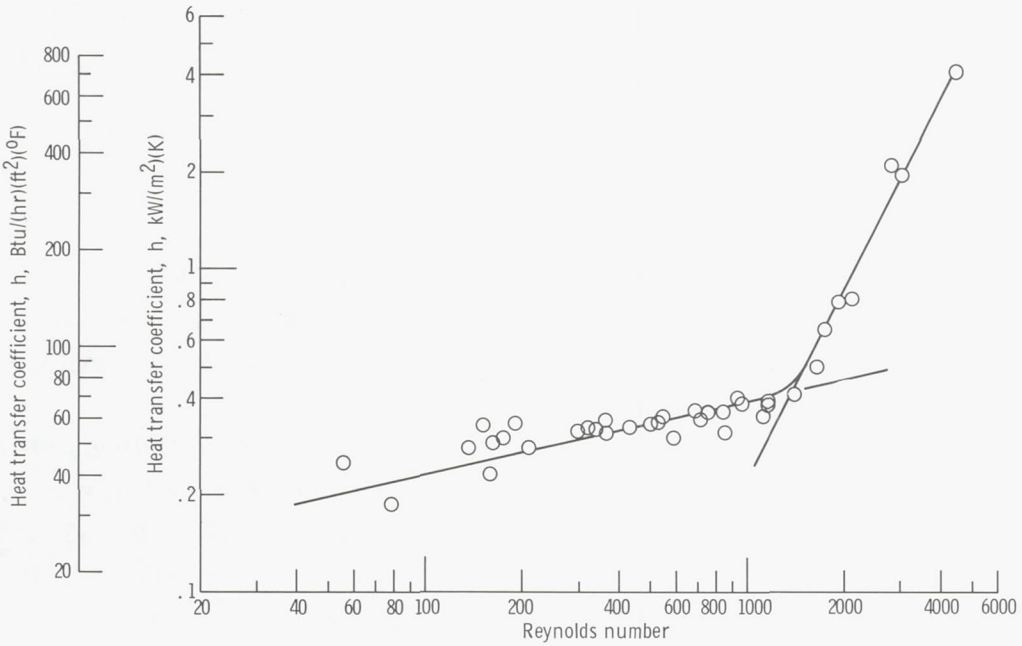

Figure 13. - Variation of heat-transfer coefficient with Reynolds number.

cient dimensionless equivalent, Nusselt number, and equating for both laminar and nonlaminar flow:

$$Nu = 1.4\,Re^{0.23} \qquad 50 < Re < 1400 \tag{12a}$$

$$Nu = 4\times10^{-6}\,Re^{2} \qquad 1400 < Re < 5000 \tag{12b}$$

The relatively minor change in Nusselt number with Reynolds number in the laminar flow range again indicates the relative independence of heat transfer on Reynolds number. The converse is true for nonlaminar flow.

Correlation to Engineering Equations

The Seider-Tate empirical equation is often referred to for estimating the overall heat transfer coefficient. This correlation at various L/D ratios is shown in figure 14. The empirical correction factor $\left(\mu_{SURFACE}/\mu\right)^{0.14}$ is essentially unity for the range of radiator tests and was not used in determining data points. Similar plots covering a Reynolds number range from 100 to 10 million and L/D ratios from 50 to 200 have been published (ref. 3).

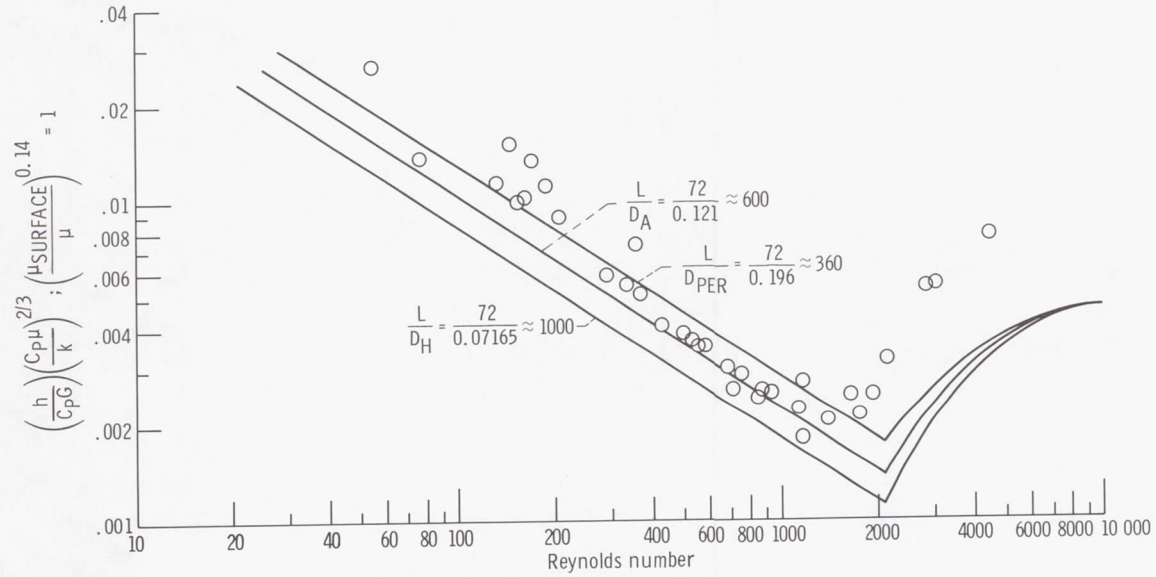

Figure 14. - Sieder-Tate heat transfer correlation at various length-diameter ratios.

As the radiator has a nonround tube geometry, three possible L/D ratios exist and are shown in figure 14. Although some texts specifically label the correlation to L/D_H ratios, test data seems to correlate best to L/D_A ratios for fully developed laminar flow. As neither the hydraulic diameter, cross-sectional equivalent diameter, nor perimeter can uniquely describe a nonround tube shape, the exactness of this correlation is questionable. For the radiator panel tube shape, the L/D ratios are not separated sufficiently to determine a specific correlation. The published curves have a maximum ordinate value of 0.0045. Test data indicate a considerably higher ordinate in the nonlaminar flow range, with only a slight indication of approaching an asymptotic value.

Other heat transfer correlations, such as using the Graetz number to correlate to a specific L/D ratio or establishing a minimum asymptotic value for Nusselt number at low flows, were not apparent from the test data and are not presented.

As the thermal conductivity of the fluid is essentially constant over the temperature range considered, a plot of Nusselt number as a function of Reynolds number is similar to figure 13, with values as listed in equations (12a) and (12b).

Panel Pressure Loss

A partial Moody diagram generated from pressure loss data is shown in figure 15. Strong correlation is evident between the predicted model for laminar flow based on hydraulic diameter and actual results for this tube configuration. Deviations from the model occur at Reynolds numbers greater than 1200. This is also the point of inflection

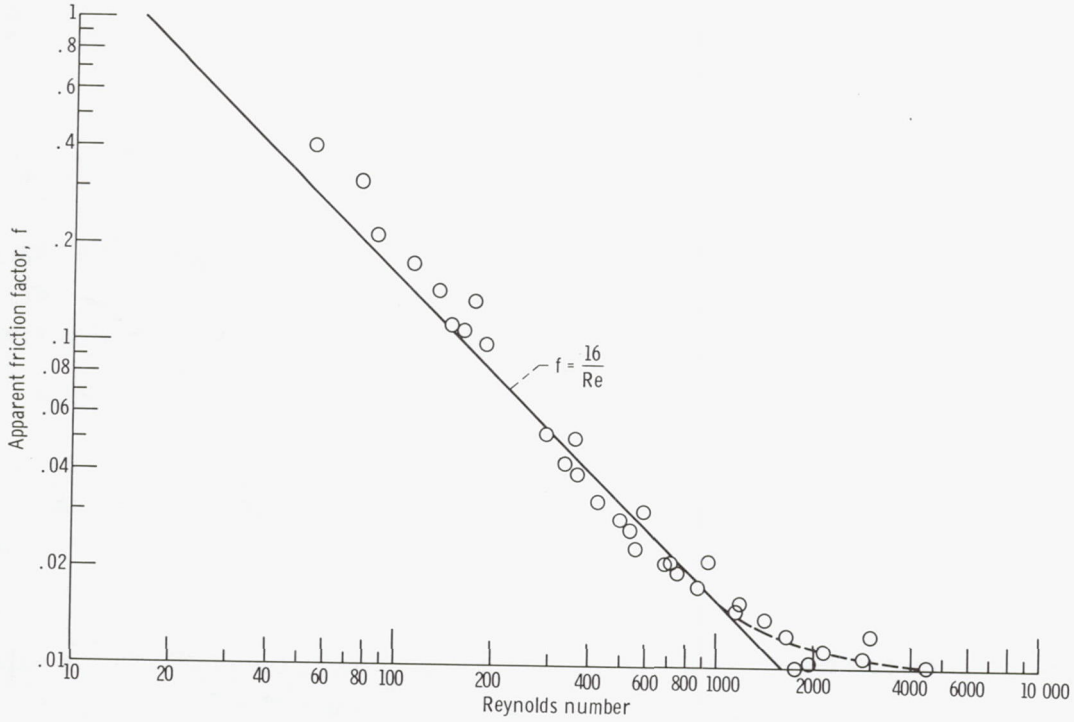

Figure 15. - Active radiator panel friction factor as function of Reynolds number. Correlation to Moody diagram in laminar flow regime.

of heat transfer properties (see fig. 13). With both heat transfer and pressure information changing at this Reynolds number, it is concluded that the transition to nonlaminar flow for this fluid begins at Reynolds numbers of 1200 to 1600.

Deviations also occur at Reynolds numbers below 200. This may be caused by a relatively thick, stationary, laminar boundary layer at the tube edges distorting the actual flow area of the tube. This effect is also the probable cause for deviations in low-flow heat transfer information in figures 13 and 14.

Actual panel pressure drop is tabulated in table III. As would be expected, pressure drop increases substantially as flow enters the nonlaminar flow regime. Pressure losses in the laminar flow regime are comparably modest.

Radiator Design Considerations

The term radiator effectiveness has generally been avoided in this report. Low-temperature radiators have a low ΔT_{FILM}; and, if combined with an adequate fin, will have a high effectiveness. As low temperature is necessary for a low ΔT_{FILM}, it also limits the amount of heat that can be rejected. Hence, high radiator efficiency is asso-

ciated with low heat-rejection rates, and the measure of a radiator is its ability to transfer heat.

Low values of ΔT_{FILM} were obtained in this program despite using a low-thermal-conductivity fluid in laminar flow. Generally, this combination is disastrous to heat transfer properties. The fact that low values of ΔT_{FILM} were obtained suggests that, for a radiator operating under similar temperatures, the fluid should be selected on its physical compatibilities with the system rather than on its heat transfer characteristics.

For maximum heat rejection, which is limited by the fluid temperature, ΔT_{FILM} must be small and fin effectiveness must be high. For high fin effectiveness, the fin material must have a high thermal conductivity. As the radiator fin becomes longer and/or thinner, its effectiveness decreases. Also, as the radiator temperature decreases, the fin effectiveness for a given fin geometry will increase.

The fluid-to-radiator-surface temperature drop decreases only slightly in laminar flow. An abrupt decrease occurs in nonlaminar flow with increasing Reynolds number (fig. 12). Operation in the nonlaminar flow regime also results in rapidly increasing pressure drop. However, ΔT_{FILM} will be small as long as the radiator temperature is low, regardless of the flow regime and the fluid.

The total heat rejected by a radiator may be increased by enlarging the perimeter area of the flow channel. If total flow area is constant, the increase in perimeter area will also reduce Reynolds number and increase the pressure drop for a given weight flow. These effects would be minimized in low-temperature laminar flow. The optimum tube configuration would depend on tradeoffs of these interrelated parameters to best fit the mission requirements.

TRANSIENT TESTS

The response of a chilled radiator to an operationally warmed fluid is shown in figure 16. This would simulate a space flight startup. Radiator positions shown are the fluid inlet and outlet and 12 center-tube temperatures. The midpanel thermocouple was slow in responding and was omitted. Data were sampled at the rate of one complete panel scan per minute. This results in each respective data point being exactly 1 minute apart rather than in a complete radiator temperature profile at any point in time.

Steady-state performance was obtained in approximately 17 minutes, with the fluid inlet temperature rising over 111 K (200^{o} F). The rapidity of radiator stabilization is attributed to the relatively low final temperature achieved and to the high thermal conductivity of aluminum. The test was performed entirely in the laminar flow region with a range of Reynolds numbers from 250 to 870 depending on the fluid temperature.

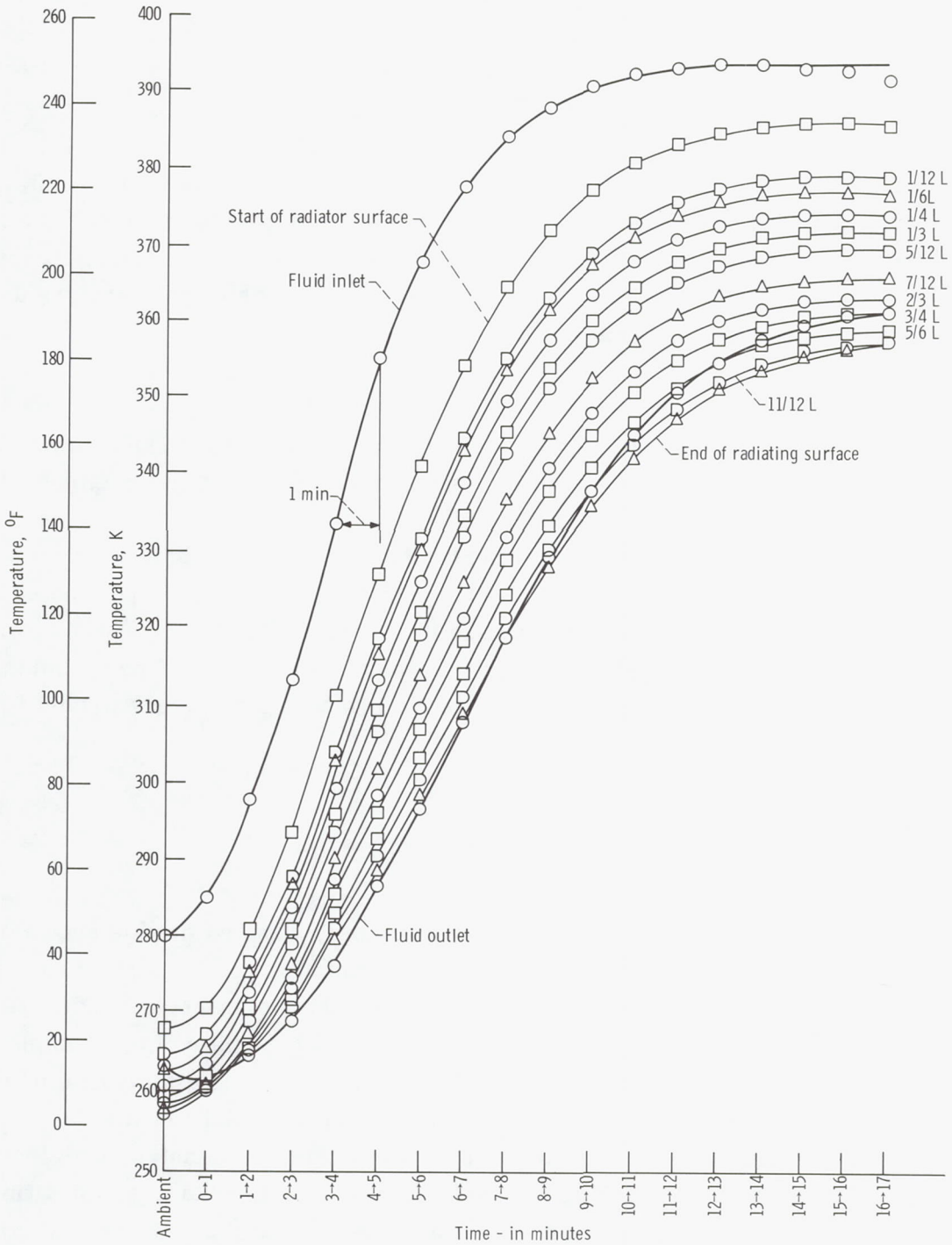

Figure 16. - Temperature profile along length of radiator with time.

CONCLUSIONS

Heat transfer and pressure drop for the D-shaped cross-section tube and the fluid used in this investigation can be predicted within engineering accuracy from existing correlations.

In laminar flow, the influence of Reynolds number on radiator efficiency is small compared to the effect of fluid temperature. Low fluid temperatures result in low heat-rejection rates per unit area and, consequently, in low temperature drop from the fluid to the radiative surface and in high radiator efficiency.

Arbitrary-shaped tubes have both a higher pressure loss and a lower Reynolds number than equivalent-area round tubes at a given mass flow rate. However, due to the increased perimeter area, the total heat-rejection rate of an arbitrary-shaped tube can be higher. The tradeoffs between increasing the perimeter area and the resulting decrease in Reynolds number appear favorable to a general low-temperature-radiator operating condition.

Lewis Research Center,
National Aeronautics and Space Administration,
Cleveland, Ohio, January 13, 1972,
112-27.

APPENDIX A

EQUATIONS FOR ARBITRARY-SHAPED TUBE

The interrelationship between a tube of nonround cross section and associated equivalent round tubes as shown in figure 3 is confusing. Here a nonround tube configuration is manipulated into four round tubes of different diameter, depending on which of four parameters is specified as being equivalent to that of the D-shaped tube. Equivalent round tubes represent correlations between fluid velocity, pressure drop, weight flow, and heat transfer area.

The relation between fluid velocity and weight flow for any tube is

$$W_T = \rho V A_T \tag{A1}$$

For a specific flow velocity, an arbitrary-shaped tube has the same Reynolds number as a round tube of equivalent hydraulic diameter.

$$Re = \frac{VD_H\rho}{\mu} \tag{10}$$

where hydraulic diameter is defined as a composite of two tube dimensions,

$$D_H = \frac{4A_T}{PER} \tag{9}$$

Reynolds number may also be equated for tubes with equivalent mass flows by combining equations (A1), (9), and (10):

$$Re = \frac{4W_T}{\mu(PER)} \tag{A2}$$

The characteristic dimension for equivalent Reynolds numbers at equivalent mass flows is the tube perimeter.

The tube perimeter also governs the heat transfer properties of the tube by the relation

$$Q = h(PER)L\ \Delta T_{FILM} \times \text{Number of tubes} \tag{6}$$

At equivalent mass flow, the relationship of equivalent pressure drop in laminar flow of a round tube to that of an arbitrary tube can be expressed by

$$D_{PRESS} = 4\sqrt[4]{\frac{A_T^3}{\pi(PER)^2}} \qquad (A4)$$

which is also a composite of two tube dimensions.

APPENDIX B

SYMBOLS

A	radiator surface area, 1.39 m^2; 15 ft^2
A'	prime radiator area, $A \times \eta$, m^2; ft^2
A_T	tube cross-sectional area, 7.42 mm^2; 0.0115 $in.^2$
C	constant, less than 1
C_P	specific heat at constant pressure, J/(kg)(K); Btu/(lbm)(^oF)
D	diameter, m; in.
D_A	diameter of round tube of equivalent cross section, $\sqrt{4A_T/\pi}$, 3.07 mm; 0.121 in.
D_H	diameter of round tube of equivalent hydraulic diameter, $4A_T/(PER)$, 1.82 mm; 0.07165 in.
D_{PER}	diameter of round tube of equivalent perimeter, 4.98 mm; 0.196 in.
D_{PRESS}	diameter of round tube of equivalent pressure drop, 2.37 mm; 0.0931 in.
F	radiative grey-body shape factor, 0.87
f	friction factor
Gr	Graetz number, WC_P/k
h	heat transfer coefficient, W/(m^2)(K); Btu/(ft^2)(hr)(^oF)
h_T	tube height, 1.22 mm; 0.048 in.
k	thermal conductivity, W/(m)(K); Btu/(ft)(hr)(^oF)
L	active radiator length, 1.83 m; 72 in.
Nu	Nusselt number, hD_H/k
P	pressure, N/m^2; $lbf/in.^2$
PER	tube perimeter, 16.3 mm; 0.642 in.
Q	total heat rejected, W; Btu/hr
Re	Reynolds number, $VD_H\rho/\mu$
T	temperature, K; ^oF
T_{CT}	effective temperature of radiative center-tube surface, K; ^oF
T_{EFF}	effective temperature of radiative fluid, K; ^oF

T_{FLUID}	temperature of bulk fluid at any point, K; ^{o}F
T_{IN}	fluid temperature at inlet, K; ^{o}F
T_{OUT}	fluid temperature at outlet; K, ^{o}F
T_{RAD}	effective temperature of radiative surface, K; ^{o}F
T_{SINK}	effective radiator sink temperature, K; ^{o}F
ΔT_{FILM}	temperature differential between bulk fluid and radiator tube surface, K; ^{o}F
V	fluid velocity, m/sec; ft/sec
W	total mass flow rate, kg/sec; lbm/hr
W_T	mass flow rate per tube, kg/sec; lbm/hr
X	distance along radiator length, m; in.
ϵ	surface hemispherical emittance, 0.93
η	efficiency, $A'/A \times 100$
μ	absolute viscosity, kg/(m)(sec); lbm/(ft)(hr)
ρ	fluid density, kg/m^3; lbm/ft^3
σ	Stefan-Boltzmann constant, 5.67×10^{-8} $W/(m^2)(K^4)$; 0.171×10^{-8} $Btu/(hr)(ft^2)(^{o}R^4)$

REFERENCES

1. Fenn, David B.; Deyo, James N.; Miller, Thomas J.; and Vernon, Richard W.: Experimental Performance of a 2-15 Kilowatt Brayton Power System in the Space Power Facility Using Krypton. NASA TM X-52750, 1970.

2. Miller, T. J.; Couch, J. P.; and Prok, G. M.: Design and Preliminary Testing of a Brayton Space Radiator Concept. Proceedings of the Intersociety Energy Conversion Engineering Conference. SAE, 1971, pp. 403-408.

3. Kreith, Frank: Principles of Heat Transfer. International Textbook Co., 1958.

TABLE I. - RADIATOR AND COLD-WALL

INSTRUMENTATION

Instrumentation	Number of instruments
Radiator panel surface thermocouples	37
Radiator fluid temperature probes (inlet and outlet)	2
Radiator fluid pressures (inlet and outlet)	2
Radiator turbine fluid flowmeters (0 to 6.3 and 0 to 30.15 cm^3/sec; 0 to 1 and 0 to 5 gal/min)	2
Cold-wall surface thermocouples	6
Cold-wall fluid probes (inlet and outlet)	2
Cold-wall fluid pressure (inlet and outlet)	2
Cold-wall turbine fluid flowmeter (0 to 163 cm^3/sec; 0 to 26 gal/min)	1

TABLE II. - NOMINAL RADIATOR DATA

SAMPLING CONDITIONS

Radiator flow rate		Fluid temperature		Cold-wall temperature	
cm^3/sec	gal/min	K	^oF	K	^oF
6.3	0.1				
12.6	.2	[a]314	105		
25.2	.4	[a]366	200		
37.8	.6	[a]414	286	250	-10
50.4	.8	[b]295	71		
63.0	1.0	[b]314	105		
126.0	2.0				

[a] T_{IN}.

[b] T_{OUT}.

TABLE III. - RADIATOR PERFORMANCE - SUMMARY OF MEASURED AND COMPUTED PARAMETERS

(a) SI units

Test	Flow		Temperature						Pressure		Heat			Reynolds number, Re
	Volume flow, cm^3/sec	Total mass flow rate, W, g/sec	Fluid inlet temperature, T_{IN}, K	Fluid outlet temperature, T_{OUT}, K	Effective temperature of radiative fluid, T_{EFF}, K	Effective temperature of radiative surface, T_{RAD}, K	Fluid-to-radiator-surface temperature differential, ΔT_{FILM}, K	Effective radiator sink temperature, ΔT_{SINK}, K	Friction factor, f, 3.78×10^{-6} $\Delta P_\rho/W^2$	Change in pressure, ΔP, N/m^2	Total heat rejected ($\epsilon = 0.93$), Q, W	Efficiency, percent	Heat transfer coefficient, h, $W/(m^2)(K)$	
1	127.4	116.5	316.07	314.03	315.04	312.7	1.7	256.8	0.001	41 370	358.2	94.7	633.8	1766
2	63.7	58.5	315.97	311.62	313.77	310.6	2.9	257.3	.018	18 750	338.0	92.7	356.4	871
3	50.4	46.3	315.97	310.98	313.44	310.4	3.0	257.0	.021	13 790	337.7	93.0	343.3	687
4	37.9	34.6	315.02	308.82	311.86	308.5	3.0	257.3	.029	10 550	321.0	92.1	326.3	501
5	25.9	23.8	314.67	305.78	310.09	306.8	2.9	257.4	.043	7 380	307.2	92.1	324.0	336
6	12.6	11.6	316.07	301.49	308.41	304.7	3.0	258.4	.110	4 480	258.6	90.6	290.0	161
7	6.3	5.9	314.64	295.42	304.34	300.5	4.2	258.4	.312	3 310	253.3	89.6	185.6	77
8	120.5	103.5	366.83	360.79	363.78	362.2	1.3	256.8	.011	38 270	883.3	97.7	2107.5	2832
9	61.2	52.5	367.00	356.61	361.71	355.0	6.0	253.6	.014	12 690	807.5	90.6	410.3	1405
10	49.2	42.3	366.78	354.84	360.68	353.3	6.6	258.5	.018	10 140	763.5	89.3	351.8	1116
11	38.5	33.1	366.48	351.51	358.78	350.8	6.9	259.3	.021	7 580	729.3	88.2	320.0	856
12	26.9	23.2	366.83	346.91	356.49	348.2	7.1	259.2	.031	5 310	699.1	87.5	301.9	586
13	11.2	9.8	356.54	328.36	341.26	334.2	5.9	259.0	.099	3 034	547.4	87.9	280.9	209
14	8.0	7.1	367.43	324.88	344.24	334.8	7.2	259.3	----	-----	553.0	84.5	233.2	157
15	106.0	99.2	298.62	296.24	297.41	295.3	1.8	256.2	.015	44 340	226.7	93.8	388.7	1166
16	63.1	59.1	299.99	297.00	298.48	296.2	2.1	257.2	.022	22 620	228.2	93.3	338.2	706
17	52.1	48.8	297.57	293.99	295.98	293.5	1.8	256.0	.024	16 960	214.7	92.6	356.9	559
18	37.9	35.2	301.85	296.63	299.18	296.7	2.2	257.6	.033	12 270	229.9	92.8	323.4	426
19	25.2	23.3	305.78	298.01	301.77	298.9	2.4	255.9	.053	8 620	253.3	92.1	316.1	292
20	11.4	10.4	312.01	297.08	304.14	300.6	2.9	256.0	.146	4 760	265.9	90.8	275.2	135
21	4.4	4.1	320.28	293.79	305.80	301.4	3.2	257.2	.402	2 000	266.2	88.7	251.9	55
22	131.8	120.3	320.49	318.09	319.29	316.8	1.5	256.4	.011	46 820	397.1	94.8	803.5	1931
23	65.0	59.3	320.54	315.73	318.10	314.8	2.9	257.9	.022	23 240	370.5	92.8	391.0	937
24	53.0	48.7	319.76	313.22	316.24	312.6	3.1	255.9	.020	14 410	361.1	92.1	360.3	751
25	37.2	34.0	322.20	313.48	317.73	313.9	3.3	256.9	.027	9 580	367.3	91.7	335.9	536
26	24.6	22.2	328.08	315.04	321.33	316.8	3.7	258.0	.040	6 070	387.2	90.5	317.2	367
27	11.4	9.9	348.53	318.31	332.36	325.9	4.4	255.8	.100	3 103	480.6	88.4	333.7	190
28	7.8	6.7	374.66	318.33	343.22	333.8	5.1	256.3	.114	1 590	556.5	84.7	332.0	147
29	131.2	106.1	413.90	404.39	409.09	406.5	1.2	258.2	.010	40 130	1571.3	97.2	4105.5	4495
30	90.2	73.2	412.47	399.33	405.78	401.8	2.2	260.5	.013	23 790	1475.5	95.5	2024.1	3014
31	63.1	50.6	416.16	399.64	407.72	400.2	5.4	262.3	.011	10 070	1437.5	91.4	813.2	2119
32	49.2	39.7	418.61	397.21	407.60	396.8	8.4	261.2	.013	6 830	1383.6	87.8	499.4	1659
33	35.3	28.4	420.55	393.08	406.29	393.6	10.3	262.4	.016	4 410	1323.2	85.6	392.7	1172
34	13.2	10.9	410.60	357.77	382.67	369.1	8.7	258.3	.052	2 000	969.1	83.0	341.0	361
35	6.7	5.4	414.34	348.11	377.77	363.9	9.2	257.7	.135	1 310	901.2	82.3	299.6	173

TABLE III. - Concluded. RADIATOR PERFORMANCE - SUMMARY OF MEASURED AND COMPUTED PARAMETERS

(b) US customary units

Test	Flow		Temperature						Pressure		Heat			Reynolds number, Re
	Volume flow, gal/min	Total mass flow rate, W, lbm/hr	Fluid inlet temperature, T_{IN}, ^{o}F	Fluid outlet temperature, T_{OUT}, ^{o}F	Effective temperature of radiative fluid, T_{EFF}, ^{o}F	Effective temperature of radiative surface, T_{RAD}, ^{o}F	Fluid-to-radiator-surface temperature differential, ΔT_{FILM}, ^{o}F	Effective radiator sink temperature, ΔT_{SINK}, ^{o}F	Friction factor, $f = 22.9\ \Delta P_{\rho}/W^2$	Change in pressure, ΔP, psia	Total heat rejected ($\epsilon = 0.93$), Q, $\frac{Btu}{hr}$	Efficiency, percent	Heat transfer coefficient, h, $\frac{Btu}{(ft)(hr)(^{o}F)}$	
1	2.02	863	109.25	105.58	107.40	103.1	3.1	2.5	0.001	6.00	1223	94.7	111.7	1766
2	1.01	433	109.08	101.25	105.11	99.4	5.2	3.5	.018	2.72	1154	92.7	62.8	871
3	.80	343	109.08	100.09	104.52	99.0	5.4	3.0	.021	2.00	1153	93.0	60.5	687
4	.60	256	107.37	96.20	101.67	95.6	5.4	3.5	.029	1.53	1096	92.1	57.5	501
5	.41	176	106.73	90.74	98.50	92.6	5.2	3.7	.043	1.07	1049	92.1	57.1	336
6	.20	86	109.25	83.01	95.47	88.8	5.4	5.5	.110	0.65	975	90.6	51.1	161
7	.10	44	106.68	72.09	88.15	81.2	7.5	5.5	.312	.48	865	89.6	32.7	77
8	1.91	767	200.62	189.76	195.13	192.3	2.3	2.6	.011	5.55	3016	97.7	371.4	2832
9	.97	389	200.93	182.22	191.41	179.4	10.8	-3.2	.014	1.84	2757	90.6	72.3	1405
10	.78	313	200.54	179.05	189.56	176.3	11.9	5.7	.018	1.47	2607	89.3	62.0	1116
11	.61	245	200.00	173.04	186.14	171.7	12.5	7.1	.021	1.10	2490	88.2	56.4	856
12	.43	172	200.62	164.76	182.01	167.0	12.7	6.9	.031	.77	2387	87.5	53.2	586
13	.18	73	182.10	131.37	154.61	141.8	10.7	6.5	.099	.44	1869	87.9	49.5	209
14	.13	52	201.70	125.12	159.96	143.0	13.0	7.0	----	----	1888	84.5	41.1	157
15	1.68	735	77.85	73.56	75.68	71.9	3.2	1.4	.015	6.43	774	93.8	68.5	1166
16	1.00	438	80.32	74.93	77.59	73.5	3.7	3.3	.022	3.28	779	93.3	59.6	706
17	.83	361	75.95	69.51	73.09	68.7	3.3	1.2	.024	2.46	733	92.6	62.9	559
18	.60	261	83.66	74.27	78.86	74.4	3.9	4.0	.033	1.78	785	92.8	57.0	426
19	.40	172	90.74	76.75	83.54	78.3	4.4	1.0	.053	1.25	865	92.1	55.7	292
20	.18	77	101.94	75.07	87.79	81.4	5.3	1.1	.146	.69	908	90.8	48.5	135
21	.07	30	116.84	69.15	90.77	82.8	5.8	3.2	.402	.29	909	88.7	44.4	55
22	2.09	891	117.22	112.90	115.05	110.6	2.7	1.8	.011	6.79	1356	94.8	141.6	1931
23	1.03	439	117.30	108.65	112.91	106.9	5.2	4.5	.022	3.37	1265	92.8	68.9	937
24	.84	361	115.19	104.12	109.56	103.0	5.5	1.0	.020	2.09	1233	92.1	63.5	751
25	.59	252	120.29	104.59	112.24	105.3	6.0	2.8	.027	1.39	1254	91.7	59.2	536
26	.39	165	130.87	107.41	118.72	110.5	6.7	4.8	.040	.88	1322	90.5	55.9	367
27	.18	73	167.69	113.28	138.57	126.9	7.9	.8	.100	.45	1641	88.4	58.8	190
28	.12	49	214.71	113.33	158.12	141.1	9.2	1.6	.114	.23	1900	84.7	58.5	147
29	2.08	786	285.35	268.24	276.69	272.1	2.1	5.1	.010	5.82	5365	97.2	723.5	4495
30	1.43	542	282.77	259.13	270.74	263.7	4.0	9.3	.013	3.45	5038	95.5	356.7	3014
31	1.00	375	289.41	259.69	274.22	260.7	9.7	12.4	.011	1.46	4908	91.4	143.3	2119
32	.78	294	293.82	255.31	274.01	254.6	15.2	10.5	.013	.99	4724	87.8	88.0	1659
33	.56	210	297.32	247.87	271.66	248.8	18.5	12.6	.016	.64	4518	85.6	69.2	1172
34	.21	81	279.41	184.32	229.14	204.7	15.6	5.3	.052	.29	3309	83.0	60.1	361
35	.10	40	286.15	166.93	220.32	195.3	16.5	4.3	.135	.19	3077	82.3	52.8	173